Quantifying and Reducing the Uncertainty of 3D Displacement Estimates from Terrestrial Laser Scanner Point Clouds

A Case Study in Alpine Geomonitoring

Nianfang SHI[1,*], **Tomislav MEDIC**[1], **Nicholas MEYER**[1], **Annelies VOORDENDAG**[1], and **Andreas WIESER**[1]

[1] *Chair of Geosensors and Engineering Geodesy, Institute of Geodesy and Photogrammetry, ETH Zurich, Zurich, Switzerland (nianfang.shi, tomislav.medic, nicholas.meyer, annelies.voordendag, andreas.wieser@geod.baug.ethz.ch)*

[*] *corresponding author*

Abstract

Terrestrial laser scanning (TLS) can offer an effective solution to geomonitoring problems by providing high-resolution point clouds, which serve as a basis for estimating dense 3D displacements. The uncertainty of such estimates, as well as the means of reducing it remain largely unexplored. We present a case study to evaluate the accuracy of TLS-based deformation estimates from an alpine monitoring campaign consisting of 6 scanning epochs between 2019 and 2022. The point clouds acquired with a Riegl VZ-4000 scanner were processed using the Feature to Feature Supervoxel-based Spatial Smoothing (F2S3) algorithm to estimate the 3D displacement vectors. We compared these vectors to sparsely distributed ground truth measurements, acquired using Global Navigation Satellite System (GNSS) stations. The results showed that, if adequately spatially averaged over large areas, the 3D vectors can be estimated with an accuracy of a few centimeters despite the long distances of up to 4 km. This corresponds to an accuracy of a few centimeters for the displacement magnitude, and a few degrees for the direction (if the magnitude is large enough for a meaningful estimate of the direction). Herein, we additionally explore several strategies to reduce the uncertainty, where temporal averaging of multiple consecutive scans from a single epoch proved to be the most promising one, while vegetation filtering and a careful selection of the registration approach indicated limitations that require further investigations.

Keywords: Geomonitoring, terrestrial laser scanning, point clouds, 3D displacement

1 Introduction

Accurately determining deformations from point clouds remains a significant challenge due to the complexity of the required data processing algorithms. Over the years, various methods have been developed, for example, Cloud-to-Cloud Comparison (C2C) (Girardeau-Montaut et al., 2005), Piecewise Alignment Method (PAM) (Teza et al., 2007), and Multiscale Model-to-Model Cloud Comparison (M3C2) (Lague et al., 2013). While these methods differ in how they determine matching points and the directions in which distances are calculated, they all rely on Euclidean-space-based correspondences to estimate displacements. For instance, M3C2 calculates displacements between correspondences in the Euclidean space along the normal vectors of locally fitted planes. It is thus sensitive to changes orthogonal to the surface, but insensitive to displacements parallel to the surface. To address this, derivatives of M3C2 have been proposed. For example, Williams et al. (2021) identified a dominant movement direction and computed displacement along it instead of relying on the surface normal. Despite these improvements, Gojcic et al. (2021) have previously shown the inherent limitation of methods relying on Euclidean-space correspondences which results in an underestimation of larger displacements.

To mitigate this, many approaches establish correspondences in feature space rather than Euclidean space, using hand-crafted or learned feature descriptors to extract geometric information and match similar features across point clouds (e.g., Rusu et al. (2009); Gojcic et al. (2018)). Following this idea, Gojcic et al. (2020) proposed the Feature to Feature Supervoxel-based Spatial Smoothing (F2S3) algorithm. F2S3 employs deep-learning-based local descriptors to extract features and establishes correspondences based on proximity in feature space. It then computes 3D displacement vectors that capture changes in unconstrained directions, not only components orthogonal to the surfaces. Using real-world data and ground truth displacements from two landslide monitoring cases with appropriate geometric structure of the point clouds, Gojcic et al. (2021) demonstrated the superior performance of F2S3 as compared to C2C and M3C2.

Despite the advancements in estimation algorithms, a remaining challenge is to quantify the achievable uncertainty of the displacement estimates. The main uncertainty sources of TLS point clouds are identified in previous studies (Soudarissanane, 2016; Friedli, 2020), but these studies focus on quantifying the quality of point clouds rather than that of displacement estimates. Displacement estimates, however, depend not only on point cloud quality but also on the quality of available features and processing algorithms. The applied algorithms can introduce additional uncertainty components or mitigate some of the existing ones. Some studies (Barbarella et al., 2017; Voordendag et al., 2023) have quantified the uncertainty of final displacement estimates, but they are limited to algorithms sensitive to only one-dimensional (1D) analysis, specifically height differences derived from digital elevation models (DEM) generated from rasterized point clouds. Hence, there remains a lack of comprehensive information on the achievable quality of three-dimensional (3D) displacement estimates derived from TLS point clouds, such as those produced using the F2S3 algorithm.

This study aims to quantify the uncertainty in F2S3 deformation estimates. Although some preliminary evaluations exist (Gojcic et al., 2020, 2021), we perform an independent and more comprehensive evaluation on a new dataset. Specifically, we apply the F2S3 algorithm to long-range TLS scans collected in the Swiss Alps and compare the estimated deformations to those obtained from GNSS. Additionally, we explore selected strategies to reduce uncertainty: (i) averaging scans or displacement vectors, (ii) filtering out vegetation, and (iii) applying an alternative registration method. By investigating these factors, we provide an evaluation of F2S3 performance and offer practical recommendations for improving TLS-based deformation monitoring.

In Section 2, we describe the details of the dataset, the methods, and the metrics used to evaluate F2S3 estimates and to reduce the uncertainty. Section 3 presents the main results, and Section 4 concludes the study with key findings and implications.

2 Methods

2.1 Data collection

The study area lies in Mattertal, Switzerland, covering an approximate area of 3 km by 2 km. The lower areas (about 1500 - 2300 m a.s.l.) are primarily covered with trees and bushes, while the higher regions consist mostly of rock debris of various sizes (Figure 1). The region contains active landslides and rock glaciers. Further details on the dataset are available in Medic et al. (2024).

Figure 1. Photo of debris at GNSS station LS12. The debris scale can be inferred by comparing it to the researchers in the center. Photo: L. Schmid, ETH Zurich.

Scans were acquired using a RIEGL VZ-4000 terrestrial laser scanner mounted on a heavy-duty tripod on the edge of a stable bedrock across the valley, see Medic et al. (2024). A meteorological station was also installed next to the TLS station. Six epochs of TLS scans were collected: July and late August 2019, July and September 2021, July and September 2022. Each epoch contains five to seven consecutive scans, acquired around 6 PM to 9 AM on the following day to mitigate the influence of atmospheric refraction (Friedli et al., 2019). The angular resolution was set to 0.005° to balance the scan duration and spatial resolution. The distance between the region of interest and the scanner ranges from 1.5 to 4 km, and the point spacing varies from 0.14 to 0.4 m depending on the range.

Several permanently tracking single- and dual-frequency GNSS stations were available in the region, installed between 2008 and 2021. The daily coordinates of these stations have standard deviations between 2 and 4 mm (Moeller et al., 2023). They are sufficiently accurate to be used as reference for assessing the accuracy of the TLS-based deformation estimates which we expected to be on the order of 1 cm or higher (Medic et al., 2024).

2.2 Data processing

We applied a plane-based ICP registration with six degrees of freedom (DoF) in RiSCAN Pro. Afterwards, deformations were estimated using the F2S3 algorithm with default parameters (Gojcic et al., 2021). To evaluate these estimates, we selected eight GNSS stations in the scanned area with sufficient temporal overlap with the TLS data. These stations were categorized into three groups based on the longest time interval for which both GNSS and TLS measurements are available, as shown in Table 1. Since F2S3 provides high-density point-wise displacement estimates, while GNSS represents single points, a direct comparison between GNSS measurements and F2S3 results was not feasible. To address this, we assumed rigid-body motion within a 25 m radius of each GNSS antenna. This radius was chosen to capture general trends near the antenna and mitigate the noise of the raw F2S3 results while being small enough to justify the assumption of uniform motion.

Table 1. Three groups of GNSS stations based on the longest time interval for which both TLS and GNSS data are available.

Time interval	Start epoch	End epoch	Stations
3 years	2019-07	2022-07	BH07, BH12, LS12
2 years	2019-07	2021-07	BH03, LS05
1 year	2021-09	2022-09	BH22, BH23, BH13

Before comparing the F2S3 outputs with GNSS results, we applied an outlier-removal step to remove 3D vectors with magnitudes greater than 10 m. The threshold was chosen because prior knowledge of the study region indicated that most displacements were within the range of a few meters (Moeller et al., 2023).

To evaluate the accuracy, we compared the directions and magnitudes obtained using F2S3 to those obtained using GNSS. We parameterized the directions in terms of dip angle and dip direction.

To quantify the precision of the magnitude estimates, the mean absolute deviation (MAD) of the magnitudes of all F2S3 vectors within the 25 m radius was calculated. Additionally, we conducted three trials to reduce the uncertainty in F2S3 estimates. They are described in the following three subsections.

2.2.1 Averaging multiple scans

The first trial was to average multiple scans acquired within each epoch. This approach was based on the following assumptions: (i) the region of interest is stable within an epoch, (ii) random variations in scans, such as those caused by instrument instability, can be mitigated by integrating multiple scans.

Two averaging strategies were applied. The first strategy consisted of averaging the point clouds from each epoch and then estimating the deformations using the averaged scans. To achieve this, after merging all original point clouds, a voxel grid with a 0.3 m resolution was created and points within each voxel were averaged. The selection of the voxel size is a trade-off between information loss and computational efficiency. The size of 0.3 m is a compromise between these two extremes and is consistent with the approximate point spacing of the original point clouds.

The second strategy consisted of computing F2S3 displacements from all possible single-scan pairs between two epochs and averaging afterwards. For example, with four scans from July 2019 and five from July 2021, 20 F2S3 displacement vectors were calculated. These vectors were then averaged without weighting to obtain the final vector. To ensure a fair comparison, each scan was downsampled using a 0.3 m voxel grid before displacement estimation.

2.2.2 Vegetation filtering

Trees and bushes in the lower regions can negatively impact displacement estimation (Franz et al., 2016). Canopy growth or wind disturbances may cause incorrect correspondences and lead to wrong estimates. Additionally, complex geometries within each laser beam footprint in forested areas can create mixed pixels and high noise, thus reducing the point cloud quality and the deformation estimation accuracy. Therefore, we expect that excluding vegetation points may improve the estimation accuracy.

To investigate this, we tested four vegetation filtering methods: the CANUPO classifier (Brodu and Lague, 2012), Cloth Simulation Filter (CSF) (Zhang et al., 2016), Simple Morphological Filter (SMRF) (Pingel et al., 2013), and a pretrained PointNet++ classifier (Qi et al., 2017). We found the PointNet++ classifier was superior in terms of visual quality scoring and computational efficiency, so we focused exclusively on this method, herein.

2.2.3 Registration algorithm

Different registration algorithms can introduce discrepancies of a few centimeters in F2S3 distances on our dataset, and ICP-based methods have shown strong performance (Laasch et al., 2023). To further investigate the impact of registration algorithms, we explored a new method in addition to the initial approach described in Section 2.2.

The new registration method involved two steps. First, the point clouds were subsampled, and features were extracted using the FPFH descriptor (Rusu et al., 2009). These were then used with RANSAC (Fischler et al., 1981) to determine correspondences and compute transformation parameters for an initial alignment. Then, this alignment was refined using the ICP algorithm (7 DoF) with the original point clouds. Unlike plane-based ICP, which requires manual input for initial alignment, the new method uses RANSAC, potentially reducing the sensitivity of the displacement estimation with respect to the quality of the initial alignment.

3 Results and Discussion

In this section, we present the results of the uncertainty quantification. Then we discuss the results of three methods for potential reduction of the uncertainties.

3.1 Uncertainty of F2S3 results

F2S3 results within a 25 m radius of eight GNSS stations, estimated from different time intervals (Table 1), were compared with GNSS observations as described in Section 2.2. The comparison results are listed in Table 2. Except for station LS05, the F2S3 estimates align well with the GNSS measurements. The median dip angle difference is 3°, median dip direction difference is 5°, and median displacement difference is 0.05 m. A large MAD occurred at BH22, the station farthest from the laser scanner, where poor feature quality left only 30 points for F2S3 analysis, leading to higher uncertainty in the estimates. Overall, the differences between the F2S3 and GNSS results align with previous findings (Gojcic et al., 2021), reaffirming the effectiveness of the F2S3 algorithm for deformation monitoring of landslides.

Angular difference and deformation magnitude are negatively correlated: Larger F2S3 displacements correspond to smaller angular differences with GNSS results. This occurs because F2S3 estimates 3D displacement vectors without explicit directional information, making angular deviations dependent on magnitude. When displacements are large, estimation errors have less impact on direction, leading to more accurate angular estimates. However, quantifying this relationship is beyond this study's scope.

The exception was station LS05, where F2S3 estimated a displacement of 1.89 m, while the GNSS measurement indicated 9.42 m. At this station, the GNSS time series showed a sudden jump of 6.04 m on May 12^{th}, 2020 (Figure 2). Additionally, inhomogeneous deformation patterns were observed in the neighborhood of LS05, see Figure 3. The rigid-body motion assumption does not hold here, with the eastern area moving slower than the western part. Moreover, gaps in the F2S3 results next to the antenna suggest excessive deformation in these areas, such that F2S3 failed to find correspondences, see also Moeller et al. (2023). No evidence suggests mistakes in GNSS or TLS measurements, so we attribute the discrepancy to the difference between the point-wise character of GNSS results versus the areal one of TLS. Further investigation is ongoing.

Table 2. Quantitative assessment of displacements estimated using GNSS and F2S3, where ϕ is the dip angle, α the dip direction, d the displacement magnitude, and Δ the difference between F2S3 and GNSS results.

Station	F2S3 points	ϕ_{GNSS} (°)	α_{GNSS} (°)	ϕ_{F2S3} (°)	α_{F2S3} (°)	$\lvert\Delta\phi\rvert$ (°)	$\lvert\Delta\alpha\rvert$ (°)	d_{GNSS} (m)	d_{F2S3} (m)	$\lvert\Delta d\rvert$ (m)	MAD (m)
LS12	7206	47	-114	38	-112	9	2	0.93	0.89	0.05	0.19
BH07	275	20	-115	22	-121	2	6	1.12	1.23	0.10	0.22
BH12	2140	23	-111	26	-113	3	2	0.81	0.86	0.05	0.19
BH03	4883	29	-112	32	-117	3	5	0.39	0.43	0.04	0.19
LS05	6556	39	-98	42	-86	3	12	9.42	1.89	7.53	0.95
BH22	30	36	-115	34	-120	2	5	0.45	0.47	0.02	1.97
BH23	439	19	-115	5	-99	14	16	0.23	0.27	0.04	0.20
BH13	411	22	-86	19	-86	3	0	4.66	4.58	0.08	0.32
Median (excl. LS05)		-	-	-	-	3	5	-	-	0.05	0.20

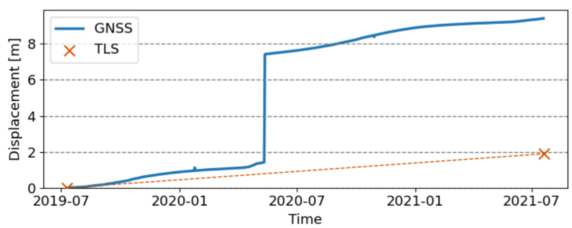

Figure 2. GNSS (blue) and TLS (orange) displacements at station LS05, with interpolated TLS displacement (dashed orange line) shown as a reference, not representing actual data.

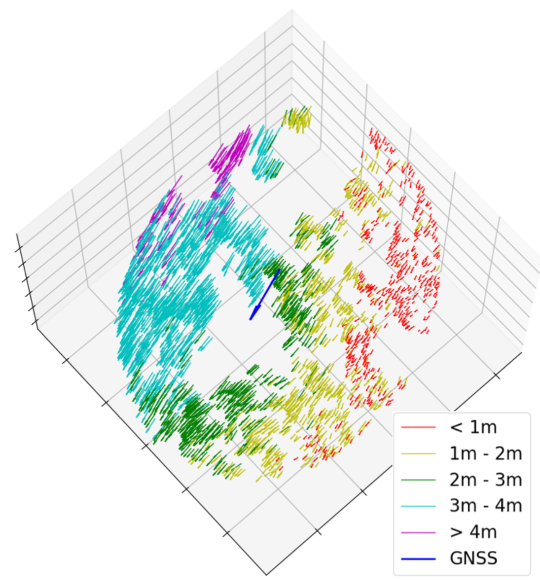

Figure 3. Visualization of F2S3 displacement vectors within 25 m of station LS05, compared to the GNSS displacement vector.

The median MAD of the F2S3 distance estimates is 0.20 m, indicating that the typical level of variation in F2S3 estimates is around 0.20 m. Stations with more F2S3 points in the neighborhood tend to have smaller MAD values. Analysis of the original point clouds shows that the number of F2S3 points largely depends on the acquired number of points around a station. Higher point densities better capture local features, producing more matched pairs and more precise deformation estimates. Our results suggest that original point density directly influences displacement estimate quality, though further investigation is needed to establish a direct relation.

3.2 Influence of averaging strategies

We can improve the accuracy and precision of the F2S3 results by estimating deformations from averaged scans. Table 3 shows results from scans averaged before correspondence search (Section 2.2.1). For simplicity, the analysis focuses only on magnitude estimates. Compared with non-averaged scans, averaging multiple scans improved the mean accuracy of the F2S3-based magnitudes from 0.05 m to 0.04 m, and the median precision from 0.20 m to 0.16 m. For most stations, the MAD decreased to between 0.16 m and 0.18 m, indicating improved precision of individual per-point magnitude estimates. These subtle but noticeable improvements in both accuracy and precision are due to reduced noise and reduced impact of quasi-random systematic effects (e.g. refraction and instrument instability) achieved through simple scan averaging.

An alternative approach, averaging F2S3 displacements after estimation, was also tested and the results are presented in Table 4. Comparing Tables 3 and 4, both strategies achieved similar accuracy. However, the second strategy resulted in worse precision, increasing the median MAD from 0.16 m to 0.22 m. Moreover, it required 20 times more computation time. These results suggest that averaging after displacement estimation is both inefficient and less effective in reducing uncertainty.

Table 3. F2S3 magnitude estimation from averaged point clouds. Symbols are defined as in Table 2.

Station	d_{F2S3} (m)	$\lvert\Delta d\rvert$ (m)	MAD (m)
LS12	0.89	0.05	0.18
BH07	1.18	0.05	0.16
BH12	0.83	0.02	0.17
BH03	0.43	0.05	0.16
BH22	0.43	0.02	0.16
BH23	0.25	0.02	0.16
BH13	4.66	0.09	0.40
Median	-	0.05	0.16

Table 4. F2S3 magnitude estimation from averaged displacements. Symbols are defined as in Table 2.

Station	d_{F2S3} (m)	$\lvert\Delta\mathrm{d}\rvert$ (m)	MAD (m)
LS12	0.89	0.04	0.20
BH07	1.19	0.06	0.22
BH12	0.83	0.02	0.20
BH03	0.42	0.04	0.20
BH22	0.45	0.00	0.25
BH23	0.25	0.02	0.24
BH13	4.70	0.13	0.38
Median	-	0.04	0.22

3.3 Influence of vegetation filtering

The results of vegetation filtering are shown in Figure 4, where green points represent vegetation and gray points indicate ground. While the pre-trained PointNet++ model effectively removed most vegetation in the lower part of the point cloud, it tended to misclassify vegetation in the upper region. This likely resulted from non-uniform point density and higher signal-to-noise ratio in the upper region, which had larger distance from the scanner. Excluding these misclassified points led to unnecessary information loss, impairing deformation monitoring in debris-covered areas.

Vegetation filtering also introduced artifacts in the displacement estimates on lower forested slopes, as shown in Figure 4. The circular patterns shown by the colors indicate unrealistic deformation estimates caused by misaligned data gaps. These gaps result from differences in vegetation point removal between point clouds. A potential solution to fix these gaps could involve smart interpolation, but further exploration is beyond the scope of this paper.

3.4 Influence of registration methods

We applied two registration methods separately (see Section 2.2.3 for details) to assess the sensitivity of deformation estimate quality to small registration changes and identify the superior method. The plane-based ICP method reduces noise through local plane estimation, while the RANSAC-integrated ICP method mitigates local minima during the transformation parameter search.

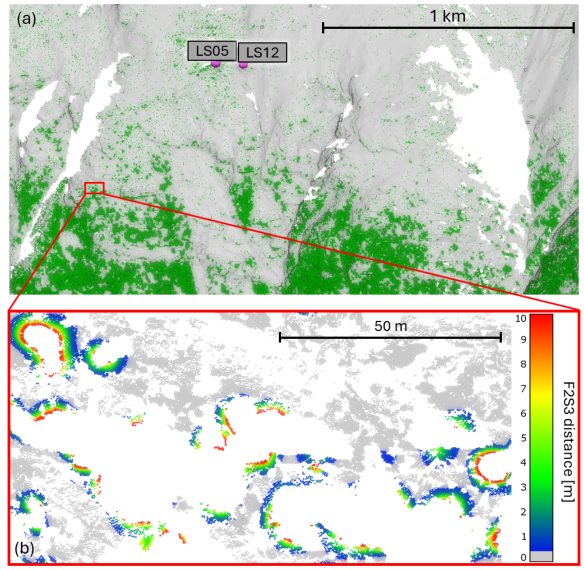

Figure 4. (a) Vegetation filtering results for the 2022-09 epoch, with vegetation (green) and ground (gray). (b) Zoomed-in view of F2S3 results (2019-07 to 2022-09) after vegetation filtering for the area within the red box.

F2S3 results from both methods are compared in Table 5. For a comprehensive comparison, we investigated both angular and magnitude estimates. F2S3 yielded similar accuracy in angular differences for both methods. However, scans registered using the RANSAC-integrated ICP method showed slightly smaller magnitude differences relative to GNSS and lower MAD values. Specifically, the median magnitude difference for the RANSAC-integrated ICP registration was 0.03 m, compared to 0.05 m for the plane-based ICP method, while the median MAD of F2S3 magnitudes was 0.19 m versus 0.20 m. These findings suggest both registration methods perform similarly, with each aligning results better with GNSS reference data for some areas. The results reaffirm that high-quality registration is key to achieving high-quality deformation estimates.

4 Conclusion

In this study, we utilized the F2S3 algorithm to estimate deformations from long-range TLS scans

Table 5. F2S3 results from different registration algorithms. Symbols are defined as in Table 2.

	RANSAC + ICP				Plane-based ICP			
Station	$\|\Delta\phi\|$ (°)	$\|\Delta\alpha\|$ (°)	$\|\Delta d\|$ (m)	MAD (m)	$\|\Delta\phi\|$ (°)	$\|\Delta\alpha\|$ (°)	$\|\Delta d\|$ (m)	MAD (m)
LS12	9	2	0.06	0.17	9	2	0.05	0.19
BH07	2	6	0.05	0.21	2	6	0.10	0.22
BH12	2	2	0.01	0.19	3	2	0.05	0.19
BH03	3	6	0.00	0.19	4	5	0.04	0.19
BH22	5	4	0.10	0.19	2	6	0.02	1.97
BH23	16	15	0.01	0.18	14	16	0.04	0.20
Median	4	5	0.03	0.19	4	6	0.05	0.20

acquired in a Swiss Alpine region and quantified the achievable accuracy and precision. Our results show that in long-range geomonitoring (up to 4 km) with an average point spacing of 0.3 m, displacement magnitudes can be estimated with an accuracy of 5 cm and individual per-point precision of about 0.2 m. Displacement direction estimates depend on magnitudes but can be accurate to within a few degrees if the magnitude exceeds about 30 cm.

We further explored the possibilities to reduce the uncertainty. Averaging scans before displacement estimation improved the accuracy and precision slightly but noticeably, while averaging after displacement estimation did not improve the quality but significantly increased the computational burden. Although this investigation is not comprehensive enough for a general conclusion, it suggests that averaging multiple scans can benefit displacement estimation in geomonitoring and should be further investigated.

In the present case, vegetation filtering introduced data gaps, causing artifacts in the deformation estimates rather than improving quality. Smart interpolation of missing ground data might be required. Two ICP-based registration methods, plane-based ICP and RANSAC-integrated ICP, achieved similar accuracy and precision in deformation estimates. The results confirm the importance of high-quality registration in reducing uncertainties in estimated displacements.

A primary limitation of the quality assessment carried out within this study is the assumption of rigid-body motion within the spherical neighborhood of 50 m diameter around each GNSS station. While this assumption holds for most of the analyzed areas, notable exceptions, such as station LS05, highlight potential biases in the deformation estimates and assessment results where this assumption is violated. We will work on algorithms that better deal with locally inhomogeneous motion patterns, both for the estimation of displacement vector fields and for quality assessment.

Acknowledgements

This study was financially supported by the Federal Office of the Environment (BAFU, grant 20.0011.PJ /6DDBCAD6D) and by the Swiss Academy of Sciences (SCNAT) through the Swiss Geodetic Commission.

References

Barbarella, M., Fiani, M., and Lugli, A. (2017). Uncertainty in terrestrial laser scanner surveys of landslides. *Remote Sensing*, 9(2):113.

Brodu, N. and Lague, D. (2012). 3D terrestrial lidar data classification of complex natural scenes using a multi-scale dimensionality criterion: Applications in geomorphology. *ISPRS Journal of Photogrammetry and Remote Sensing*, 68:121–134.

Fischler, M. A., View Profile, Bolles, R. C., and View Profile (1981). Random sample consensus. *Communications of the ACM*, 24(6):381–395.

Franz, M., Carrea, D., Abellan, A., Derron, M.-H., and Jaboyedoff, M. (2016). Use of targets to track 3D displacements in highly vegetated areas affected by landslides. *Landslides*, 13:821–831.

Friedli, E. (2020). *Point Cloud Registration and Mitigation of Refraction Effects for Geomonitoring Using Long-Range Terrestrial Laser Scanning*. PhD thesis, ETH Zurich, Zurich.

Friedli, E., Presl, R., and Wieser, A. (2019). Influence of atmospheric refraction on terrestrial laser scanning at long range. In *Proceedings of the*

4th Joint International Symposium on Deformation Monitoring (JISDM), Athens, Greece.

Girardeau-Montaut, D., Roux, M., Marc, R., and Thibault, G. (2005). Change detection on points cloud data acquired with a ground laser scanner. *International Archives of Photogrammetry, Remote Sensing and Spatial Information Sciences*, 36(3):W19.

Gojcic, Z., Schmid, L., and Wieser, A. (2021). Dense 3d displacement vector fields for point cloud-based landslide monitoring. *Landslides*, 18(12):3821–3832.

Gojcic, Z., Zhou, C., and Wieser, A. (2018). Learned compact local feature descriptor for TLS-based geodetic monitoring of natural outdoor scenes. *ISPRS Annals of the Photogrammetry, Remote Sensing and Spatial Information Sciences*, IV-2:113–120.

Gojcic, Z., Zhou, C., and Wieser, A. (2020). F2S3: Robustified determination of 3D displacement vector fields using deep learning. *Journal of Applied Geodesy*, 14(2):177–189.

Laasch, H., Jacquemart, M., Ruttner, P., Wieser, A., and Medic, T. (2023). Finding the Best TLS Point Cloud Registration Algorithm for Long-Range Geomonitoring. In *Ingenieurvermessung 23: Beiträge zum 20. Internationalen Ingenieurvermessungskurs*, pages 173 – 177, Zurich, Switzerland.

Lague, D., Brodu, N., and Leroux, J. (2013). Accurate 3D comparison of complex topography with terrestrial laser scanner: Application to the Rangitikei canyon (N-Z). *ISPRS Journal of Photogrammetry and Remote Sensing*, 82:10–26.

Medic, T., Shi, N., Meyer, N., and Wieser, A. (2024). Geomonitoring Using Long-Range TLS in Swiss Alps. In *SIG 2024 - Proceedings of the International Symposium on Engineering Geodesy*, pages 19–28, Zagreb, Croatia.

Moeller, G., Medic, T., Aichinger-Rosenberger, M., Schmid, L., Wieser, A., and Rothacher, M. (2023). Alpine Metrology Lab: Geomonitoring Using Long-Range TLS and Permanent GNSS. In *Ingenieurvermessung 23: Beiträge zum 20. Internationalen Ingenieurvermessungskurs*, pages 107–113, Zurich, Switzerland.

Pingel, T. J., Clarke, K. C., and McBride, W. A. (2013). An improved simple morphological filter for the terrain classification of airborne LIDAR data. *ISPRS Journal of Photogrammetry and Remote Sensing*, 77:21–30.

Qi, C. R., Yi, L., Su, H., and Guibas, L. J. (2017). PointNet++: deep hierarchical feature learning on point sets in a metric space. In *Proceedings of the 31st International Conference on Neural Information Processing Systems*, pages 5105–5114, New York, USA.

Rusu, R. B., Blodow, N., and Beetz, M. (2009). Fast Point Feature Histograms (FPFH) for 3D registration. In *2009 IEEE International Conference on Robotics and Automation*, pages 3212–3217, Kobe, Japan.

Soudarissanane, S. S. (2016). *The geometry of terrestrial laser scanning; identification of errors, modeling and mitigation of scanning geometry*. PhD thesis, TU Delft, Delft.

Teza, G., Galgaro, A., Zaltron, N., and Genevois, R. (2007). Terrestrial laser scanner to detect landslide displacement fields: a new approach. *International Journal of Remote Sensing*, 28(16):3425–3446.

Voordendag, A., Goger, B., Klug, C., Prinz, R., Rutzinger, M., Sauter, T., and Kaser, G. (2023). Uncertainty assessment of a permanent long-range terrestrial laser scanning system for the quantification of snow dynamics on Hintereisferner (Austria). *Frontiers in Earth Science*, 11.

Williams, J. G., Anders, K., Winiwarter, L., Zahs, V., and Höfle, B. (2021). Multi-directional change detection between point clouds. *ISPRS Journal of Photogrammetry and Remote Sensing*, 172:95–113.

Zhang, W., Qi, J., Wan, P., Wang, H., Xie, D., Wang, X., and Yan, G. (2016). An Easy-to-Use Airborne LiDAR Data Filtering Method Based on Cloth Simulation. *Remote Sensing*, 8(6):501.